Water-Based Bi2S3 Nano-Inks Obtained with Surfactant-Assisted Liquid Phase Exfoliation and Their Direct Processing into Thin Films

colloids and interfaces

MDPI

Article

Water-Based Bi_2S_3 Nano-Inks Obtained with Surfactant-Assisted Liquid Phase Exfoliation and Their Direct Processing into Thin Films

Micaela Pozzati [1], Felix Boll [2], Matteo Crisci [2], Sara Domenici [1], Francesco Scotognella [1], Bernd Smarsly [2], Teresa Gatti [1,2,*] and Mengjiao Wang [1,*]

[1] Dipartimento Scienza Applicata e Tecnologia (DISAT), Politecnico di Torino, Corso Duca degli Abruzzi 24, 10129 Torino, Italy; micaela.pozzati@polito.it (M.P.); sara.domenici@polito.it (S.D.); francesco.scotognella@polito.it (F.S.)
[2] Center for Materials Research (LaMa), Justus Liebig University, Heinrich-Buff-Ring 17, 35392 Giessen, Germany; felix.boll@phys.chemie.uni-giessen.de (F.B.); matteo.crisci@phys.chemie.uni-giessen.de (M.C.); bernd.smarsly@phys.chemie.uni-giessen.de (B.S.)
* Correspondence: teresa.gatti@polito.it (T.G.); mengjiao.wang@polito.it (M.W.)

Abstract: Bi_2S_3 has gained considerable attention as a semiconductor for its versatile functional properties, finding application across various fields, and liquid phase exfoliation (LPE) serves as a straightforward method to produce it in nano-form. Till now, the commonly used solvent for LPE has been N-Methyl-2-pyrrolidone, which is expensive, toxic and has a high boiling point. These limitations drive the search for more sustainable alternatives, with water being a promising option. Nonetheless, surfactants are necessary for LPE in water due to the hydrophobic nature of Bi_2S_3, and organic molecules with amphoteric characteristics are identified as suitable surfactants. However, systematic studies on the use of ionic surfactants in the LPE of Bi_2S_3 have remained scarce until now. In this work, we used sodium dodecyl sulfate (SDS), sodium dodecylbenzene sulfonate (SDBS) and sodium hexadecyl sulfonate (SHS) as representative species and we present a comprehensive investigation into their effects on the LPE of Bi_2S_3. Through characterizations of the resulting products, we find that all surfactants effectively exfoliate Bi_2S_3 into few-layer species. Notably, SDBS demonstrates superior stabilization of the 2D layers compared to the other surfactants, while SHS becomes the most promising surfactant for obtaining products with high yield. Moreover, the resulting nano-inks are used for fabricating films using spray-coating, reaching a fine tuning of band gap by controlling the number of cycles, and paving the way for the utilization of 2D Bi_2S_3 in optoelectronic devices.

Keywords: Bi_2S_3; surfactant-assisted liquid phase exfoliation; nano-ink; spray-coating

Citation: Pozzati, M.; Boll, F.; Crisci, M.; Domenici, S.; Scotognella, F.; Smarsly, B.; Gatti, T.; Wang, M. Water-Based Bi_2S_3 Nano-Inks Obtained with Surfactant-Assisted Liquid Phase Exfoliation and Their Direct Processing into Thin Films. *Colloids Interfaces* **2024**, *8*, 28. https://doi.org/10.3390/colloids8030028

Received: 29 February 2024
Revised: 23 April 2024
Accepted: 24 April 2024
Published: 30 April 2024

1. Introduction

Metal chalcogenides cover a large family of 2D materials, which have gained recent attention due to their potential significance in many technological applications [1–6]. Among them, Bi_2S_3 emerges as a potential candidate in thermoelectric applications, energy harvesting, biomedicine, sensors and optoelectronics, due to its low thermal conductivity, strong spin-orbit coupling, direct band structure and high absorption coefficient [7–12]. As shown in Figure 1a, Bi_2S_3 possesses a lamellar structure in which the bismuth and sulfur atoms are bonded through strong covalent bonds inside the layer, and these layers are linked by van der Waals (vdW) forces to one another [13]. This unique layered structure allows the vdW interactions between layers in bulk Bi_2S_3 to be broken by mechanical force, thus producing 2D layered Bi_2S_3.

Liquid phase exfoliation (LPE) is a simple and scalable technique used to produce 2D layered materials. This procedure consists of delaminating the layers of the material dispersed in a solvent by mechanical force. In sonication-assisted LPE, the sonication generates the growth and collapse of microbubbles in the solvents, thus resulting in shock waves. These waves can exert shear forces on bulk materials, disrupt the vdW interactions between the layers of the 2D structures and ultimately lead to the formation of layered materials [14–16]. The type of solvent plays an important role in the efficiency of the exfoliation, and the solvent typically used for exfoliating Bi_2S_3 is N-methyl-2-pyrrolidone (NMP) [17–20]. Considering the high cost, high boiling point and toxicity of NMP, replacing it with water has become a more eco-friendly and sustainable strategy.

Since Bi_2S_3 is hydrophobic, surfactants are needed to separate and stabilize the nanocrystals in H_2O. In LPE, the frequently used surfactants are anionic surfactants that can counteract vdW attraction between the material layers, inhibiting restacking by electrostatic force with each single layer [21,22]. One of the most employed surfactants for metal chalcogenides is the anionic surfactant sodium dodecyl sulfate (SDS), and its structure is shown in Figure 1b [23,24]. The molecule contains an anion with C_{12} alkyl chain and SO_4^- group on the terminal of the carbon chain. The carbon chains construct semi-micelles on the basal plane of metal chalcogenides to prevent the restacking of the exfoliated nanosheets, while the terminal SO_4^- group forms a H-bond with water and stabilizes the exfoliated layers [25]. Our previous work also proves the possibility of exfoliation of Bi_2S_3 with SDS [26]. Moreover, surfactants with a similar structure to SDS but different functional groups have been reported in LPE, such as sodium dodecylbenzene sulfonate (SDBS). It has been reported that the benzene ring in SDBS improves the colloidal stability of exfoliated MoS_2 [27]. Furthermore, it has been reported that by changing the alkyl chain length, the stability of the exfoliated suspension and optoelectronic property of the colloidal nanocrystals can be optimized as well [28]. However, a study regarding the influence of the carbon chain of the surfactant on the LPE process is still missing. In addition to the type of surfactant, the concentration of the surfactant significantly influences the quality and yield of exfoliated metal chalcogenides [21,29]. Therefore, surfactant concentration will be a crucial parameter in optimizing the harvesting of exfoliated Bi_2S_3 with good quality and high yield.

Based on the above background knowledge, in this work we systematically investigate how surfactant type and concentration impact the quality of exfoliated Bi_2S_3. Three different surfactants have been chosen, SDS, SDBS and sodium hexadecyl sulfate (SHS), to compare the influence of different functional groups and carbon chain lengths on the LPE of Bi_2S_3 (Figure 1). It has been reported that controlling the concentration of the surfactants less than their critical micelle concentration (CMC) can result in better-quality exfoliated samples, while other studies reached contradictory conclusions [30,31]. In our study, we set the concentrations from 8.2 mM to 0.5 mM for all the surfactants for better comparison, considering that the CMCs of SDS, SDBS and SHS are 8.2, 2.7 and 0.55 mM, respectively [32–35]. By assessing the band gap, stability and yield of the exfoliated Bi_2S_3, it is found that SHS results in the largest band gap and yield, while the colloidal suspension is more stable with SDBS. As to the influence of the concentration, a higher concentration of all the surfactants tends to form exfoliated samples with a higher band gap. Only SHS shows a correlation between the concentration and the sample yield, and the record yield of 1.4% is obtained with 8.2 mM SHS. Moreover, concentration does not influence the stability of the suspension. Eventually, we also show that the suspension can be made into Bi_2S_3 thin films with a tunable band gap through ultrasonic spray-coating, which is a promising perspective for the use of these nano-inks in the field of eco-friendly, solution-processed optoelectronics.

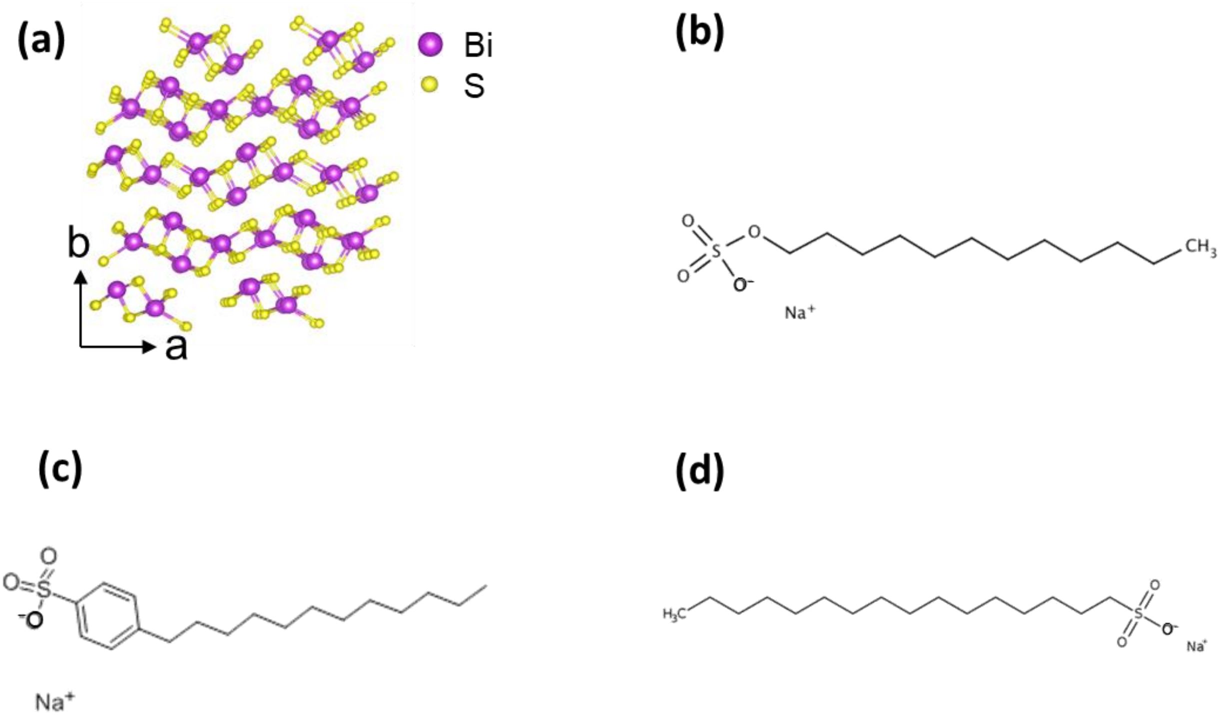

Figure 1. (**a**) Crystalline structure of Bi_2S_3 along the *c*-axis highlighting the vdW architecture and molecular structures of (**b**) SDS, (**c**) SDBS and (**d**) SHS.

2. Materials and Methods

2.1. Materials and LPE Process

Fluorine-doped tin oxide (FTO) coated glass slides, Bi_2S_3 (99%), SDS and SDBS were purchased from Sigma Aldrich and used without further purification. SHS was purchased from TCI Chemicals and used without further purification. All the exfoliations were performed using a Baudelin Sonopuls tip sonicator and the samples were cooled to 0 °C with an ice bath during the process. The tip sonicator operated with 80% power using pulses of 1 s on/1 s off for 4 h.

In all the experiments, the suspension volume was 150 mL with a concentration of the bulk materials of 10 mg/mL. The concentrations of all the surfactants were adjusted to 8.2 mM, 4.1 mM, 2.0 mM, 1.0 mM and 0.5 mM, respectively. The suspensions obtained after the sonication were centrifuged firstly for 30 min at 1500 rpm to reserve the supernatant, then this supernatant was centrifuged for 30 min at a higher speed of 3000 rpm to obtain the final colloidal suspensions. A Universal 320 Hettich centrifuge was employed for the centrifuge treatment.

Thin Bi_2S_3 films were fabricated using the Nadetech Innovations Ultrasonic Lab Spray Coater on FTO glass substrates measuring 15 × 15 mm, and the suspensions from the previous steps were directly used as inks for the spray-coating. We used N_2 pressure with 0.10 bar to get a uniform spray. The speed of the nozzle was 400 mm/min, and the working flow of the suspension was 25 mL/h.

2.2. Characterizations

UV-visible (UV-vis) absorption spectra of the colloidal suspensions were captured using a Goebel Uvikon spectrometer, employing a quartz cuvette with an optical length of 1 cm. The spectra were recorded from 350 to 1000 nm with a scan interval of 0.25 nm. Raman spectra were acquired using a Bruker Senterra instrument equipped with a 532 nm laser excitation source at a power of 2 mW. Integration time was set to 6 s with 60 co-additions. Samples were prepared by drop-casting suspensions onto silicon slides for analysis. Dynamic Light Scattering (DLS) and Zeta potential (ZP) measurements were conducted on a Malvern Zetasizer Nano-ZS device, averaging results from three separate measurements for accuracy. Measurements were performed in Rotilabo precision glass cuvettes with a light path of 10 mm and a volume of 3.5 mL. High-Resolution Transmission Electron Microscopy (HRTEM) imaging was performed using a non-aberration-corrected Transmission Electron Microscope (TALOS F200X, Thermo Scientific, Eindhoven, The Netherlands) operating at 200 kV. Images were captured using a 16Mpxls CMOS camera with an exposure time of 1 s. The fast Fourier transform (FFT) pattern was converted with the Velox software (Thermo Scientific Velox Software, Thermo Fisher Scientific Inc., Waltham, MA, USA).

2.3. Calculation Methods of the Sample Concentration

UV-vis spectra were employed to calculate the final concentration of Bi_2S_3. A calibration line was obtained using a set of dilutions from a suspension with a known concentration, and this concentration of samples was obtained using filtration of the products. The slope of the calibration line corresponds to the extinction coefficient of the dispersed material. The final concentrations of Bi_2S_3 samples were obtained with the Lambert-Beer law (Equation (1)):

$$A = \varepsilon bc \quad (1)$$

where A represents the absorbance of the material, ε denotes the extinction coefficient of the dispersed nanosheets, and c signifies the concentration of the suspension. Specifically, we utilized the absorption value at 500 nm as A. The value of ε is derived from calibration lines established using several standard Bi_2S_3 suspensions with known concentrations. For Bi_2S_3, the calculated ε is determined to be 7.4 mg/mL·cm.

To compare with the concentration calculated from UV-vis spectra, freeze-drying was used to obtain the final concentration as well. Before freeze-drying, dialysis was performed using a cellulose dialysis bag (Carl Roth) 14 kDa, filling each bag with 20–25 mL of the desired suspension and closing both sides with a plastic pin once filled. The bag was then left in a suitable beaker with Milli-Q water for 3 days, changing the water 3 times per day. Freeze-drying was performed at −10 °C for 16 h and at a pressure of 1 mPa.

3. Results and Discussion

3.1. Characterizations of the Resulting Nanomaterials

3.1.1. TEM Analysis

The exfoliated Bi_2S_3 nano-inks were prepared using the surfactant-assisted LPE method outlined in Section 2.1 and a typical exfoliated Bi_2S_3 sample was used to characterize the morphology and crystal structure of the colloids. As depicted in Figure 2a–c, nanosheets of irregular shapes are observed, predominantly appearing as a few layers of around 10 nm of thickness rather than single layers. The size distribution of the exfoliated samples ranges from 50 to 350 nm, with the size of around 150–200 nm as the dominate value (Figure S1). Study of the selected area electron diffraction (SAED) illustrates that the crystalline nanosheets can be indexed to orthorhombic structured Bi_2S_3 (ICSD: 30775) (Figure 2d). Figure 2e,f depict the HRTEM image and its corresponding FFT pattern, revealing lattice planes within the nanosheets. These planes exhibit spacings of 0.79 nm and 0.36 nm, indicative of the 101 and 301 planes, respectively. This small nanosheet shows a [010] orientation, since it is possible to break the bulk Bi_2S_3 in the direction of [010] to obtain nanoribbons (Figure 1a) [31].

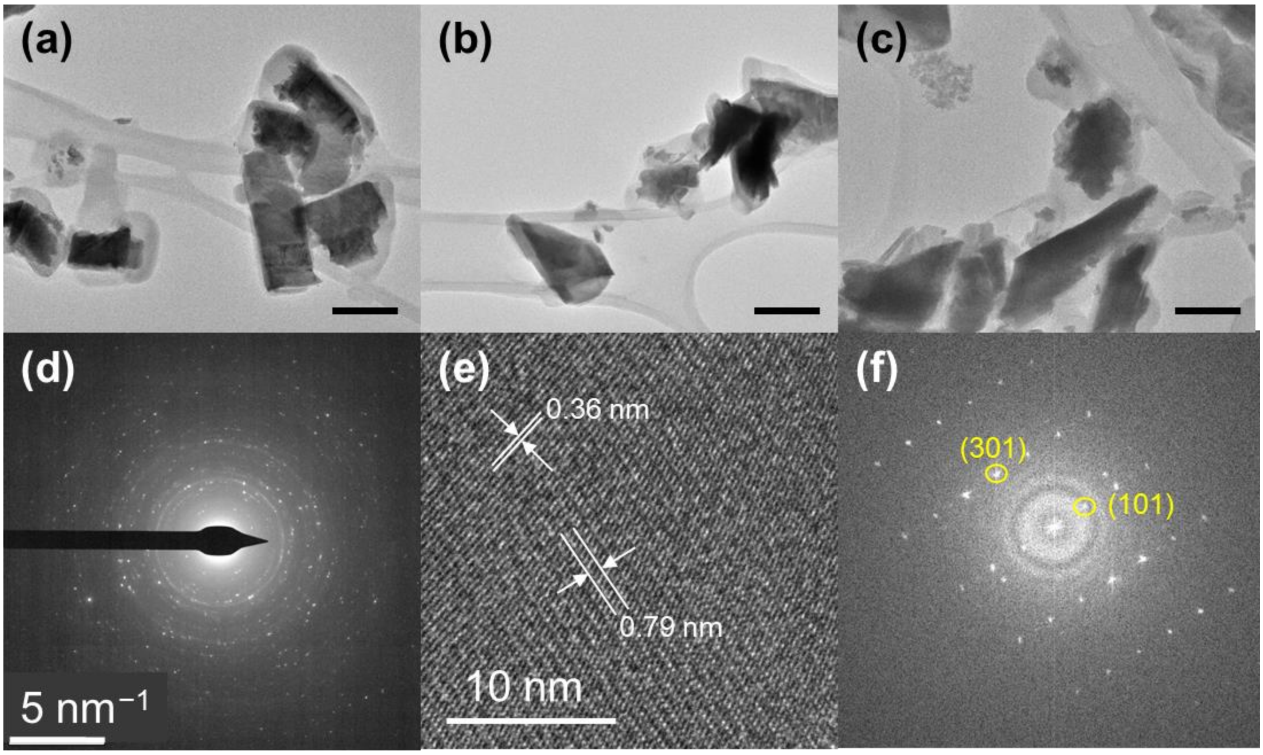

Figure 2. TEM image of exfoliated Bi_2S_3 with (**a**) SDS, (**b**) SDBS and (**c**) SHS. The scale bar in each panel is 200 nm. (**d**) SAED pattern and (**e**) HRTEM of typical Bi_2S_3 nanosheets. (**f**) is the FFT pattern of region (**e**).

3.1.2. UV-vis Analysis

Figure 3a–c show the UV-vis absorption spectra of Bi_2S_3 samples exfoliated with different types and concentrations of surfactants. It can be observed that there is a growing absorption intensity when the wavelength decreases for all the samples [21,22]. In samples with the highest surfactant concentration, there is a notable rapid decline in absorption intensity beyond 550 nm. This phenomenon could likely be attributed to the strong influence exerted by the elevated concentration of surfactants (Figure S2). As a consequence, this high concentration of surfactant gives less scattering in the spectrum. The band gap of all the samples was calculated with the Tauc Plot equation (Equation (2)):

$$(\alpha hv)^{1/n} = A\ (hv - E_g) \quad (2)$$

where α is the absorption coefficient, h is the Plank constant, v is the frequency, E_g is the band gap energy and n is 1/2 for Bi_2S_3 with a direct band gap [36]. The values are shown in Figure 3d–f and Table 1. In general, all the samples have a broader band gap ranging from 1.74 to 2.44 eV in comparison to the band gap of bulk Bi_2S_3 (1.3 eV) [37]. This is evidence that all the samples were exfoliated to nanoscale. Regarding the impact of surfactant type, SDS yielded nano-inks with a lower band gap ranging from 1.85 to 2.03 eV, whereas samples with SHS exhibited a higher band gap range of 2.08 to 2.3 eV. This indicates that samples derived from SHS possess a smaller size in terms of thickness or particle size. Concerning surfactant concentration, the overarching trend is that higher concentrations lead to broader band gaps. It is worth noting the detected non-linear change in band gap with surfactant concentration. This complexity arises from various factors influencing the band gap: not only is it connected to quantum confinement effects, but it is also significantly impacted by the atomistic arrangement on the nanosheet surface, which is dictated by the nature of the capping surfactant [28]. Though higher concentrations are not strictly related to higher band gap, all these concentrations still result in samples with a widened band gap, which is proof that all the concentrations can exfoliate bulk Bi_2S_3.

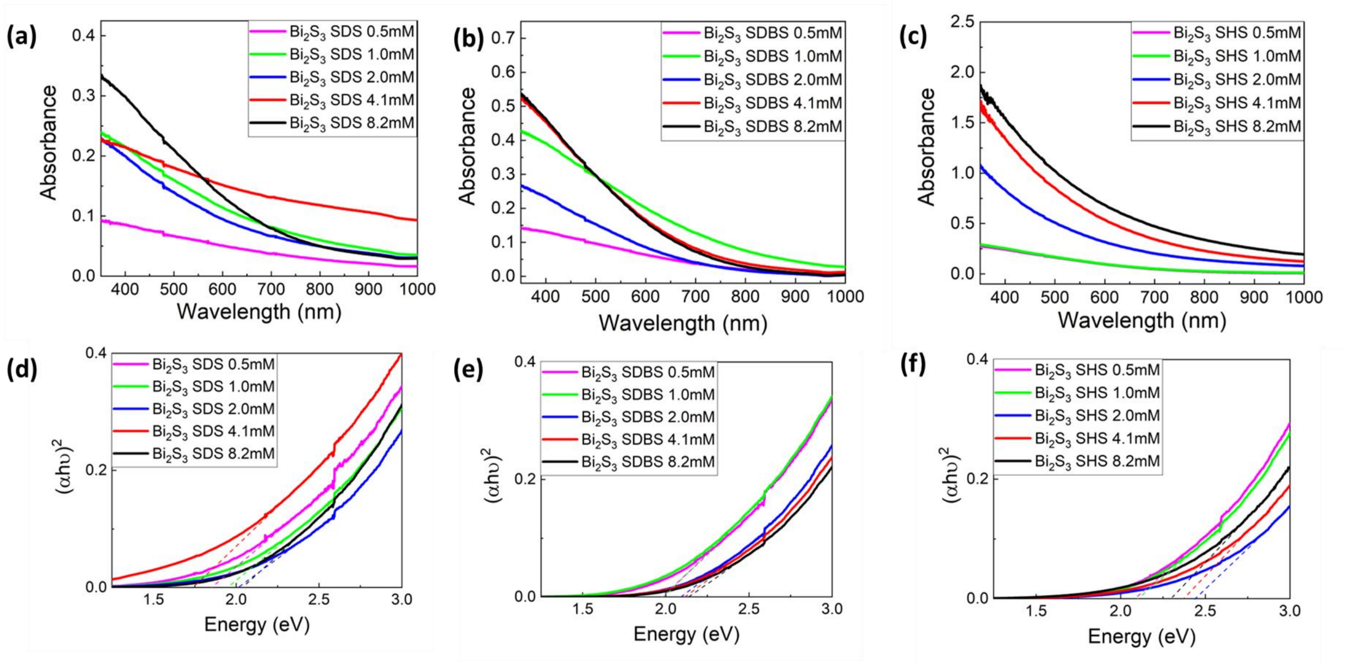

Figure 3. UV-vis absorption spectra and corresponding Tauc plots of exfoliated Bi_2S_3 nano-inks with (**a**,**d**) SDS, (**b**,**e**) SDBS and (**c**,**f**) SHS.

Table 1. Optical band gap values extrapolated from Tauc plots of all exfoliated Bi_2S_3 nano-inks.

Surfactant	Surf. Concentration (mM)	Band Gap (eV)
SDS	8.2	2.03
	4.1	1.74
	2.0	2.01
	1.0	1.95
	0.5	1.85
SDBS	8.2	2.13
	4.1	2.11
	2.0	2.10
	1.0	1.99
	0.5	1.97
SHS	8.2	2.30
	4.1	2.37
	2.0	2.44
	1.0	2.10
	0.5	2.08

3.1.3. Raman Analysis

Figure 4 displays the Raman spectra of Bi_2S_3 samples with all the surfactants. It is possible to identify two main active modes, namely the B_{1g} and A_g Raman modes, in all the samples. The peaks located at 188 cm^{-1} and 237 cm^{-1} belong to B_{1g} mode, which arises from longitudinal vibrations, while the A_g transversal modes are noticeable at 106 cm^{-1}, 170 cm^{-1} and 265 cm^{-1} [38] After the exfoliation of the material, the frequency of the longitudinal optical phonon is higher, so the ratio between the two modes decreases [39]. The two modes with the most identifiable peaks (B_{1g} mode at 237 cm^{-1} and A_g mode at 265 cm^{-1}) were chosen to characterize the surficial property of the exfoliated samples. Specifically, the intensity ratio of A_g mode and B_{1g} mode is calculated to determine whether the samples were exfoliated [19,40]. In bulk Bi_2S_3, the A_g/B_{1g} ratio is 1.68 [26], while for all the exfoliated Bi_2S_3, the A_g/B_{1g} ratio ranges from 1.02 to 1.32 (Table 2), which is clear evidence that all the samples were exfoliated, and the surficial molecular vibration modes are different from the bulk Bi_2S_3. When comparing band gap values with A_g/B_{1g} ratios in Raman spectra, a linear correlation is not emerging. Initially, a lower ratio of A_g/B_{1g} suggests a higher band gap, yet this association is due to the quantum confinement effect, which is related to layer count, nanosheet anisotropy and average size. In these experiments, the average size of the nanosheets is not controlled, thus it is difficult to build a linear relationship between the average number of layers and the band gap values. However, there is no report in the literature related to the values of A_g/B_{1g} ratio and its connection to any layer property of exfoliated Bi_2S_3, thus we do not obtain any further information from Raman spectra. Concerning the Raman mode shift in the samples, a distinct shift compared to bulk Bi_2S_3 was not observed, except for Bi_2S_3 SDBS 8.2 mM. This is likely due to the fact that the frequency of the Raman mode does not vary significantly whether Bi_2S_3 is in bulk form or exfoliated. Another prominent mode observed in the samples using SDBS appears at around 122 cm^{-1}. This mode corresponds to a Bi-O stretching characteristic of β-Bi_2O_3, which may be associated with a non-stable oxide phase likely induced by laser irradiation [41].

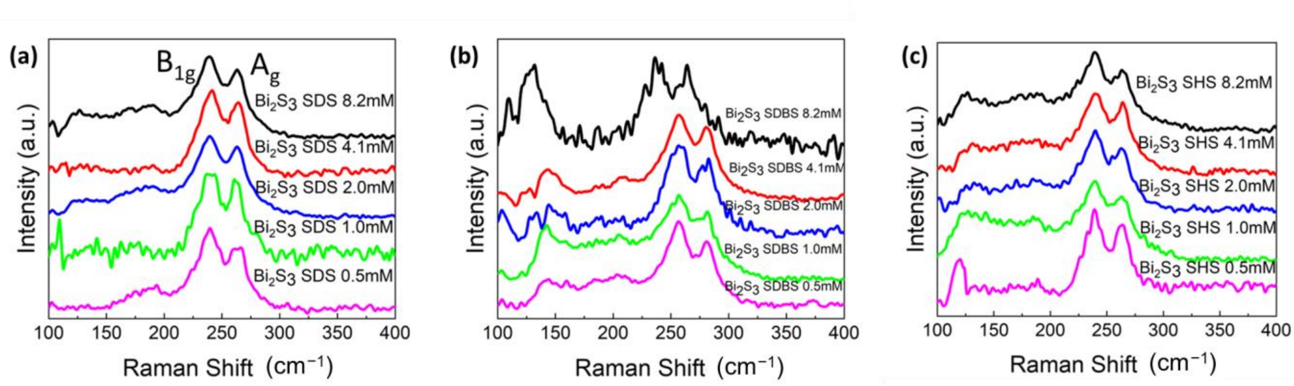

Figure 4. Raman spectra of Bi_2S_3 (**a**) SDS, (**b**) SDBS and (**c**) SHS.

Table 2. A_g/B_{1g} ratio of all Bi_2S_3 samples.

2D Material	Surfactant	Surf. Concentration (mM)	A_g/B_{1g} Ratio
Bi_2S_3	SDS	8.2	1.20
		4.1	1.18
		2.0	1.15
		1.0	1.07
		0.5	1.32
Bi_2S_3	SDBS	8.2	1.32
		4.1	1.25
		2.0	1.19
		1.0	1.17
		0.5	1.02
Bi_2S_3	SHS	8.2	1.30
		4.1	1.12
		2.0	1.30
		1.0	1.25
		0.5	1.25

3.1.4. Zeta Potenzial and DLS

ZP analysis was conducted to evaluate the stability of the Bi_2S_3 colloidal suspensions from the surfactant-assisted LPE method. Generally, when the ZP values are between −20 and −30 mV, the suspension shows a short-term stability, while samples with −30 mV ZP values show a long-term stability of up to several months [42]. Figure 5a illustrates that all Bi_2S_3 water-based inks exhibit a ZP value below −30 mV, indicating long-term colloidal stability of more than one month. Specifically, the ZP values of most Bi_2S_3 samples are in the range between −30 and −50 mV, and the surfactant concentration appears to have minimal impact on them. An exceptional value of −80 mV is observed for the ink produced using 8.2 mM of SDBS, indicating that the colloidal suspension obtained under these experimental conditions exhibits outstanding stability.

The average particle size of each sample was estimated by DLS and the results are shown in Figure 5b. The average particle size of Bi_2S_3 remains approximately 100 nm for SDBS, and the particle size shows a slight decrease when the surfactant concentration increases. Upon comparing the concentration with the obtained band gap values, a positive correlation becomes evident. Higher band values correspond to increased surfactant concentration, resulting in a slight reduction in the average particle size. The sizes range from approximately 110 nm to 90 nm, spanning surfactant concentrations of 0.5 to 8.2 mM, respectively. With SDS, the average particle size of Bi_2S_3 ranges from around 200 nm to 125 nm from the lowest to highest surfactant concentration and it drops dramatically when increasing the concentration of SDS. It is apparent that some inconsistencies emerge in band gap values versus average particle size calculated from DLS. This discrepancy may arise from the fact that for 2D and 1D materials, DLS primarily estimates the lateral length of the nanosheet rather than the thickness [43]. Since both small thickness and small lateral length of the nanosheets correspond to higher band gap values, because of the quantum confinement, the influence of layer thickness is not considered in the values of DLS, thus causing the mismatch between band gap values and average particle size, as measured from DLS. Additionally, surface chemistry can influence band gap values as well, and this factor has not been well studied for exfoliated Bi_2S_3 with surfactants yet. Meanwhile, the trend in particle size using SHS shows a rough range mostly under 200 nm, but little correlation with the concentration of SHS and band gap values, as shown in Figure S3. This trend in particle size agrees with the result from the band gap calculation in Table 1, in which we expect samples with SDS to have roughly larger size than samples with SDBS.

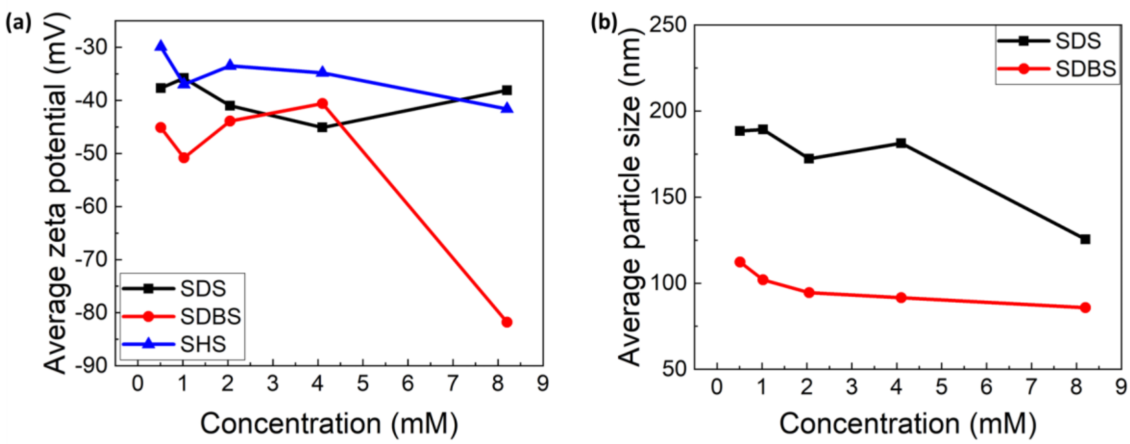

Figure 5. Zeta potential (**a**) and DLS (**b**) trends for the exfoliated Bi_2S_3 nano-inks.

3.2. Yield and Final Concentration of the Nanomaterials

The yield of the exfoliated material is another crucial metric used to evaluate the effects of the surfactants and the associated experimental variables. As described in Section 2.3, UV-vis spectra are employed to quantify the final concentration of the samples. All the results are listed in Table 3 and shown in Figure 6. Apparently, samples with SHS demonstrate superior values compared to those treated with the other two surfactants. Especially with surfactant concentrations higher than 2.0 mM, the concentration of SHS reaches more than 0.05 mg/mL and yields more than 0.5%, while all the samples obtained with SDS and SDBS have a concentration lower than this value. Moreover, higher SHS concentration can result in higher yield, and we are able to obtain the maximum sample concentration of 0.14 mg/mL and yield of 1.4% in this work with 8.2 mM of SHS.

To validate this data, selected samples with higher concentrations were subjected to freeze-drying after removing the surfactant through dialysis, and different values compared to the calculated concentration from UV-vis spectra were obtained. This is probably due to the residual presence of surfactant in the dispersion or the loss of samples during the operation.

Table 3. Product concentration and yield for LPE Bi_2S_3 calculated from Lambert-Beer law and from weighted freeze-dried samples.

Surfactant	Surfactant Concentration (mM)	Product Concentration with UV-vis Absorption (mg/mL)	Product Concentration with Freeze-Drying (mg/mL)	Yield (%)
SDS	8.2	0.03		0.3
	4.1	0.02		0.2
	2.0	0.02		0.2
	1.0	0.02		0.2
	0.5	0.01		0.1
SDBS	8.2	0.04	0.04	0.4
	4.1	0.04		0.4
	2.0	0.02		0.2
	1.0	0.04		0.4
	0.5	0.01		0.1
SHS	8.2	0.14	0.08	1.4
	4.1	0.11	0.44	1.1
	2.0	0.07		0.7
	1.0	0.02		0.2
	0.5	0.02		0.2

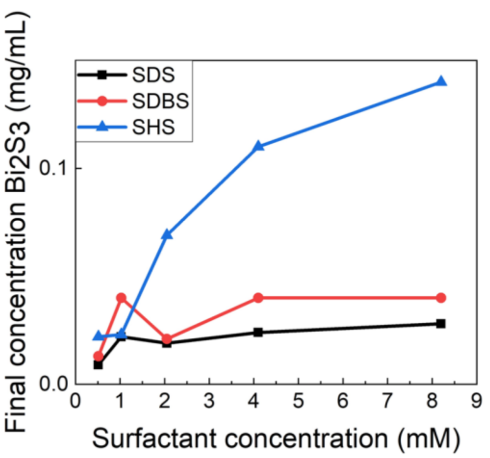

Figure 6. Final concentration exfoliated Bi_2S_3 nano-inks.

3.3. Production of Thin Films with Ultrasonic Spray-Coating

To test the potential for solution-processing of the prepared, water-based nano-inks, we produced thin films of Bi_2S_3 using the ultrasonic spray-coating method, which is very suitable for deposition of nanomaterial inks and might pave the way to potential applications of these colloids in the sustainable fabrication of optoelectronic devices. With the Bi_2S_3 nano-ink exfoliated with 2.0 mM of SDBS, we sprayed for multiple steps on transparent substrates, to be able to detect the change in band gap as a function of the number of layers deposited. The colloidal ink was directly used without further dilution, since the concentration of the product was already very low (0.02 mg/mL). Figure 7 shows the UV-vis spectra of the thin films prepared from spraying exfoliated Bi_2S_3. From the corresponding Tauc plots, the band gap values of the Bi_2S_3 thin films are found to be 1.43 and 1.26 eV for 30 and 50 spray-steps, respectively (Figure 7b). The intense absorption is consistent with the remarkable extinction coefficient of Bi_2S_3 [44]. Furthermore, the absorption spectrum is clearly characterized by fringes. These fringes are evidently due to the FTO film between the glass substrate and Bi_2S_3 thin films. In fact, it is remarkable that, for the two different Bi_2S_3 thin films, the spectral position of the fringes is the same. It is evident that by adjusting the number of sprayed layers, the tuning of the band gap of the Bi_2S_3 film is possible. These values are smaller than the band gaps of the nanosheets in the suspension (Table 1), which is likely due to the nanosheets aggregation at the solid state, within the film. Figure 7c,d display the SEM images of the as-synthesized thin films. In Figure 7d, after 50 layers of spray coating, the sample shows a uniform Bi_2S_3 surface, while the sample with 30 layers is not fully covering the transparent conductive oxide substrate. The full-view images of Figure 7c,d are shown in Figure S4.

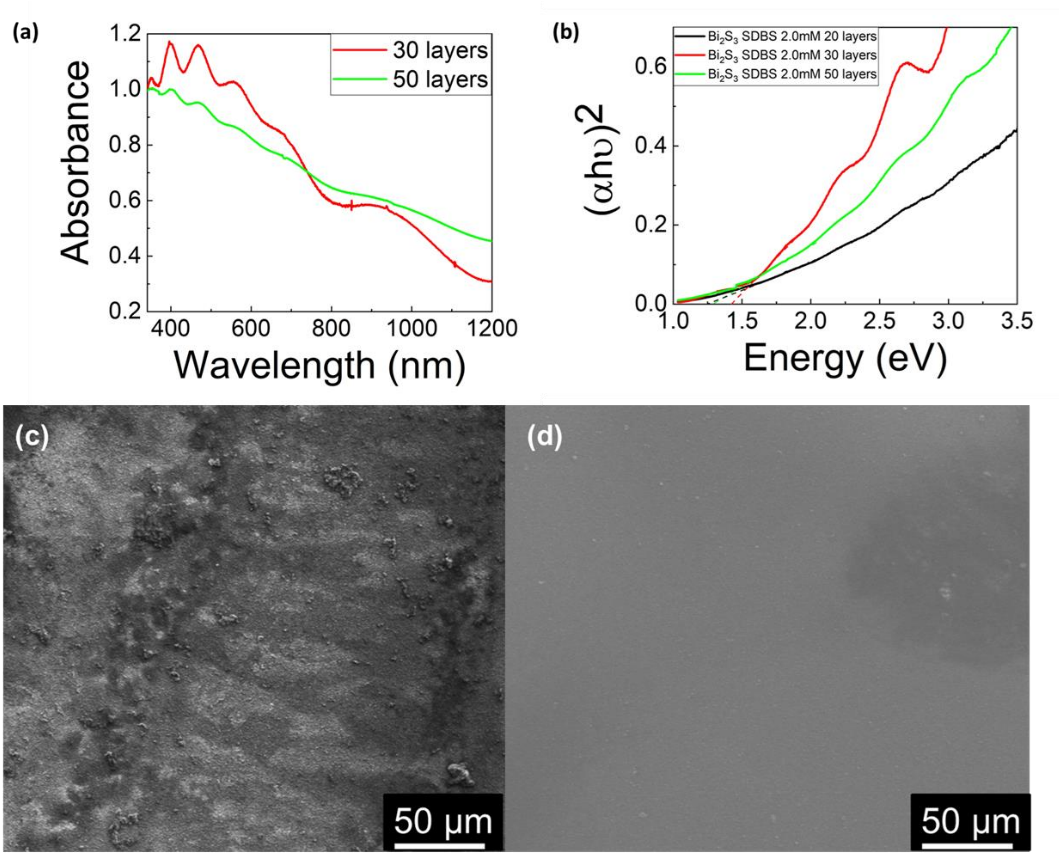

Figure 7. (**a**) UV-vis spectra and (**b**) Tauc Plot of Bi_2S_3 thin films produced from multiple ultrasonic spray-coating steps from the 2 mM SDBS nano-ink. Top-view SEM images of the Bi_2S_3 thin films with (**c**) 30 and (**d**) 50 sprayed layers.

4. Conclusions

In conclusion, we conducted a systematic investigation into the surfactant-assisted LPE of Bi_2S_3. Utilizing three distinct ionic surfactants (SDS, SDBS and SHS), we performed exfoliation processes in water to generate stable colloidal suspensions, through a green method that is a good alternative to the use of toxic organic solvents. Through comprehensive characterization employing various techniques, we compared the quality of the exfoliated 2D Bi_2S_3 nanosheets present in the inks in terms of layer size, colloidal stability and product yield. It is found that with SHS, an exfoliated Bi_2S_3 with smaller particle size and higher yield can be obtained, but SDBS can lead to more stable colloidal suspensions compared to the other two surfactants investigated. Moreover, SHS with higher concentrations results in a higher yield in the exfoliated product, with the 8.2 mM concentration providing the optimal value of 1.4%. Considering that the CMC of SHS is only 0.55 mM, our results surprisingly indicate that the best concentration is high above the value of CMC. Moreover, we found that uniform Bi_2S_3 films with a tunable band gap can be obtained with ultrasonic spray-coating, while further optimization of the film fabrication process is needed to obtain films for practical applications in optoelectronic devices.

Supplementary Materials: The following supporting information can be downloaded at: https://www.mdpi.com/article/10.3390/colloids8030028/s1, Figure S1: Histogram of the distribution of particle size Bi_2S_3; Figure S2: UV-vis spectrum of SDS 8.2mM; Figure S3: DLS Bi_2S_3 SHS; Figure S4: SEM images of the Bi_2S_3 thin films with (a) 30 (b) 50 layers. Table S1: Parameters of LPE process.

Author Contributions: Conceptualization, T.G. and M.W.; methodology, M.P., F.B., S.D. and M.C.; software, M.P.; validation, M.P. and M.W.; formal analysis, M.P., M.C., F.S. and F.B; investigation, M.W.; resources, B.S. and T.G.; data curation, M.P.; writing—original draft preparation, M.P.; writing—review and editing, M.W., T.G. and F.S.; supervision, M.W.; project administration, B.S. and T.G.; funding acquisition, T.G. and M.W. All authors have read and agreed to the published version of the manuscript.

Funding: This research was funded by the ERC StG project JANUS BI (grant agreement No. [101041229]) and by the Starting Grant ERC program of Compagnia di San Paolo.

Data Availability Statement: The data from this study are available upon request made to the corresponding author.

Acknowledgments: M.W. and T.G. thank Fondazione Compagnia di San Paolo for financial support through the "Bando TRAPEZIO—Paving the way to research excellence and talent attraction". M.C. and F.B. acknowledge the support of the European Commission through the H2020 FET-PROACTIVE-EIC-07-2020 project LIGHT-CAP (grant number 101017821).

Conflicts of Interest: The authors declare no conflicts of interest.

References

1. Shawky, A.; Alahmadi, N.; Mohamed, R.M.; Zaki, Z.I. Bi_2S_3-Sensitized TiO_2 Nanostructures Prepared by Solution Process for Highly Efficient Photoreduction of Hexavalent Chromium Ions in Water Under Visible Light. *Opt. Mater.* **2022**, *124*, 111964. https://doi.org/10.1016/j.optmat.2021.111964.
2. Ott, S.; Wolff, N.; Rashvand, F.; Rao, V.J.; Zaumseil, J.; Backes, C. Impact of the MoS_2 Starting Material on the Dispersion Quality and Quantity after Liquid Phase Exfoliation. *Chem. Mater.* **2019**, *31*, 8424–8431. https://doi.org/10.1021/acs.chemmater.9b02336.
3. Han, M.; Jia, J. The Interlace of Bi_2S_3 Nanowires with TiO_2 Nanorods: An Effective Strategy for High Photoelectrochemical Performance. *J. Colloid Interface Sci.* **2016**, *481*, 91–99. https://doi.org/10.1016/j.jcis.2016.07.045.
4. Zhang, X.; Shi, Y.; Shi, Z.; Xia, H.; Ma, M.; Wang, Y.; Huang, K.; Wu, Y.; Gong, Y.; Fei, H.; et al. High-Pressure Synthesis of Single-Crystalline SnS Nanoribbons. *Nano Lett.* **2023**, *23*, 7449–7455. https://doi.org/10.1021/acs.nanolett.3c01879.
5. Barraza-Lopez, S.; Fregoso, B.M.; Villanova, J.W.; Parkin, S.S.P.; Chang, K. Colloquium: Physical Properties of Group-IV Monochalcogenide Monolayers. *Rev. Mod. Phys.* **2021**, *93*, 011001. https://doi.org/10.1103/RevModPhys.93.011001.
6. Villanova, J.W.; Kumar, P.; Barraza-Lopez, S. Theory of Finite-Temperature Two-Dimensional Structural Transformations in Group-IV Monochalcogenide Monolayers. *Phys. Rev. B* **2020**, *101*, 184101. https://doi.org/10.1103/PhysRevB.101.184101.
7. Xie, Y.; Zhou, Y.; Gao, C.; Liu, L.; Zhang, Y.; Chen, Y.; Shao, Y. Construction of AgBr/BiOBr S-Scheme Heterojunction Using Ion Exchange Strategy for High-Efficiency Reduction of CO_2 to CO under Visible Light. *Sep. Purif. Technol.* **2022**, *303*, 122288. https://doi.org/10.1016/j.seppur.2022.122288.

8. Bai, Y.; Ouyang, T.; Li, X.; Yan, Y.; Kong, Z.; Ma, X.; Li, Z.; Li, Z.; Cai, X.; Cai, J.; et al. Boosting the Thermoelectric Performance of n-Type Bi_2S_3 by Compositing rGO. *J. Alloy. Compd.* **2023**, *933*, 167814. https://doi.org/10.1016/j.jallcom.2022.167814.
9. Zhao, F.; Sheng, H.; Sun, Q.; Wang, J.; Liu, Q.; Hu, Z.; He, B.; Wang, Y.; Li, Z.; Liu, X. Harvesting the Infrared Part of Solar Light to Promote Charge Transfer in Bi_2S_3/WO_3 Photoanode for Enhanced Photoelectrochemical Water Splitting. *J. Colloid Interface Sci.* **2022**, *621*, 267–274. https://doi.org/10.1016/j.jcis.2022.04.052.
10. Xu, Y.; Chen, B.; Xu, L.; Zhang, G.; Cao, L.; Liu, N.; Wang, W.; Qian, H.; Shao, M. Urchin-like Fe_3O_4@Bi_2S_3 Nanospheres Enable the Destruction of Biofilm and Efficiently Antibacterial Activities. *ACS Appl. Mater. Interfaces* **2023**, *16*, 3215–3231. https://doi.org/10.1021/acsami.3c17888.
11. Zamani, M.; Jamali-Sheini, F.; Cheraghizade, M. Visible-Range and Self-Powered Bilayer p-Si/n-Bi_2S_3 Heterojunction Photodetector: The Effect of Au Buffer Layer on the Optoelectronics Performance. *J. Alloy. Compd.* **2022**, *905*, 164119. https://doi.org/10.1016/j.jallcom.2022.164119.
12. Yang, Z.; Wang, Y.; Zhang, D.; Chen, C. A Sensitizing Photoelectrochemical Sensing Platform Strategy Based on Bio-Etching Preparation of Bi_2S_3/BiOCl p–n Heterojunction. *Talanta* **2018**, *190*, 357–362. https://doi.org/10.1016/j.talanta.2018.08.004.
13. Smith, R.J.; King, P.J.; Lotya, M.; Wirtz, C.; Khan, U.; De, S.; O'Neill, A.; Duesberg, G.S.; Grunlan, J.C.; Moriarty, G.; et al. Large-Scale Exfoliation of Inorganic Layered Compounds in Aqueous Surfactant Solutions. *Adv. Mater.* **2011**, *23*, 3944–3948. https://doi.org/10.1002/adma.201102584.
14. Li, Z.; Young, R.J.; Backes, C.; Zhao, W.; Zhang, X.; Zhukov, A.A.; Tillotson, E.; Conlan, A.P.; Ding, F.; Haigh, S.J.; et al. Mechanisms of Liquid-Phase Exfoliation for the Production of Graphene. *ACS Nano* **2020**, *14*, 10976–10985. https://doi.org/10.1021/acsnano.0c03916.
15. Xu, Y.; Cao, H.; Xue, Y.; Li, B.; Cai, W. Liquid-Phase Exfoliation of Graphene: An Overview on Exfoliation Media, Techniques, and Challenges. *Nanomaterials* **2018**, *8*, 942. https://doi.org/10.3390/nano8110942.
16. Sarkar, A.S.; Konidakis, I.; Gagaoudakis, E.; Maragkakis, G.M.; Psilodimitrakopoulos, S.; Katerinopoulou, D.; Sygellou, L.; Deligeorgis, G.; Binas, V.; Oikonomou, I.M.; et al. Liquid Phase Isolation of SnS Monolayers with Enhanced Optoelectronic Properties. *Adv. Sci.* **2023**, *10*, 2201842. https://doi.org/10.1002/advs.202201842.
17. Jawaid, A.; Nepal, D.; Park, K.; Jespersen, M.; Qualley, A.; Mirau, P.; Drummy, L.F.; Vaia, R.A. Mechanism for Liquid Phase Exfoliation of MoS_2. *Chem. Mater.* **2016**, *28*, 337–348. https://doi.org/10.1021/acs.chemmater.5b04224.
18. Hu, C.X.; Shin, Y.; Read, O.; Casiraghi, C. Dispersant-Assisted Liquid-Phase Exfoliation of 2D Materials beyond Graphene. *Nanoscale* **2021**, *13*, 460–484. https://doi.org/10.1039/D0NR05514J.
19. Guo, Y.; Zhao, Q.; Yao, Z.; Si, K.; Zhou, Y.; Xu, X. Efficient Mixed-Solvent Exfoliation of Few-Quintuple Layer Bi_2S_3 and Its Photoelectric Response. *Nanotechnology* **2017**, *28*, 335602. https://doi.org/10.1088/1361-6528/aa79ce.
20. Sarkar, A.S.; Stratakis, E. Dispersion Behaviour of Two Dimensional Monochalcogenides. *J. Colloid Interface Sci.* **2021**, *594*, 334–341. https://doi.org/10.1016/j.jcis.2021.02.081.
21. Griffin, A.; Nisi, K.; Pepper, J.; Harvey, A.; Szydłowska, B.M.; Coleman, J.N.; Backes, C. Effect of Surfactant Choice and Concentration on the Dimensions and Yield of Liquid-Phase-Exfoliated Nanosheets. *Chem. Mater.* **2020**, *32*, 2852–2862. https://doi.org/10.1021/acs.chemmater.9b04684.
22. Ying, G.G. Fate, Behavior and Effects of Surfactants and their Degradation Products in the Environment. *Environ. Int.* **2006**, *32*, 417–431. https://doi.org/10.1016/j.envint.2005.07.004.
23. Gupta, A.; Arunachalam, V.; Vasudevan, S. Water Dispersible, Positively and Negatively Charged MoS_2 Nanosheets: Surface Chemistry and the Role of Surfactant Binding. *J. Phys. Chem. Lett.* **2015**, *6*, 739–744. https://doi.org/10.1021/acs.jpclett.5b00158.
24. Domínguez, H. Self-Aggregation of the SDS Surfactant at a Solid-Liquid Interface. *J. Phys. Chem. B* **2007**, *111*, 4054–4059. https://doi.org/10.1021/jp067768b.
25. Yu, H.; Zhu, H.; Dargusch, M.; Huang, Y. A Reliable and Highly Efficient Exfoliation Method for Water-Dispersible MoS_2 Nanosheet. *J. Colloid Interface Sci.* **2018**, *514*, 642–647. https://doi.org/10.1016/j.jcis.2018.01.006.
26. Wang, M.; Crisci, M.; Pavan, M.; Liu, Z.; Gallego, J.; Gatti, T. New Insights into the Surfactant-Assisted Liquid-Phase Exfoliation of Bi_2S_3 for Electrocatalytic Applications. *Catalysts* **2023**, *13*, 551. https://doi.org/10.3390/catal13030551.
27. Guan, Z.; Wang, C.; Li, W.; Luo, S.; Yao, Y.; Yu, S.; Sun, R.; Wong, C.P. A Facile and Clean Process for Exfoliating MoS_2 Nanosheets Assisted by a Surface Active Agent in Aqueous Solution. *Nanotechnology* **2018**, *29*, 425702. https://doi.org/10.1088/1361-6528/aad676.
28. Zhang, B.; Wang, M.; Ghini, M.; Melcherts, A.E.M.; Zito, J.; Goldoni, L.; Infante, I.; Guizzardi, M.; Scotognella, F.; Kriegel, I.; et al. Colloidal Bi-Doped $Cs_2Ag_{1-x}Na_xInCl_6$ Nanocrystals: Undercoordinated Surface Cl Ions Limit Their Light Emission Efficiency. *ACS Mater. Lett.* **2020**, *2*, 1442–1449. https://doi.org/10.1021/acsmaterialslett.0c00359.
29. Lotya, M.; King, P.J.; Khan, U.; De, S.; Coleman, J.N. High-Concentration, Surfactant-Stabilized Graphene Dispersions. *ACS Nano* **2010**, *4*, 3155–3162. https://doi.org/10.1021/nn1005304.
30. Abreu, B.; Almeida, B.; Ferreira, P.; Fernandes, R.M.F.; Fernandes, D.M.; Marques, E.F. A Critical Assessment of the Role of Ionic Surfactants in the Exfoliation and Stabilization of 2D Nanosheets: The Case of the Transition Metal Dichalcogenides MoS_2, WS_2 and $MoSe_2$. *J. Colloid Interface Sci.* **2022**, *626*, 167–177. https://doi.org/10.1016/j.jcis.2022.06.097.
31. Wang, S.; Yi, M.; Shen, Z. The Effect of Surfactants and Their Concentration on the Liquid Exfoliation of Graphene. *RSC Adv.* **2016**, *6*, 56705–56710. https://doi.org/10.1039/c6ra10933k.
32. Markarian, S.A.; Harutyunyan, L.R.; Harutyunyan, R.S. The Properties of Mixtures of Sodium Dodecylsulfate and Diethylsulfoxide in Water. *J. Solution Chem.* **2005**, *34*, 361–368. https://doi.org/10.1007/s10953-005-3056-x.

33. Yang, K.; Zhu, L.; Xing, B. Enhanced Soil Washing of Phenanthrene by Mixed Solutions of TX100 and SDBS. *Environ. Sci. Technol.* **2006**, *40*, 4274–4280. https://doi.org/10.1021/es060122c.
34. Muzzalupo, R.; Gente, G.; La Mesa, C.; Caponetti, E.; Chillura-Martino, D.; Pedone, L.; Saladino, M.L. Micelles in Mixtures of Sodium Dodecyl Sulfate and a Bolaform Surfactant. *Langmuir* **2006**, *22*, 6001–6009. https://doi.org/10.1021/la052863h.
35. Antonioli Júnior, R.; Poloni, J.d.F.; Pinto, É.S.M.; Dorn, M. Interdisciplinary Overview of Lipopeptide and Protein-Containing Biosurfactants. *Genes* **2023**, *14*, 76. https://doi.org/10.3390/genes14010076.
36. Messalea, K.A.; Zavabeti, A.; Mohiuddin, M.; Syed, N.; Jannat, A.; Atkin, P.; Ahmed, T.; Walia, S.; McConville, C.F.; Kalantar-Zadeh, K.; et al. Two-Step Synthesis of Large-Area 2D Bi_2S_3 Nanosheets Featuring High In-Plane Anisotropy. *Adv. Mater. Interfaces* **2020**, *7*, 2001131. https://doi.org/10.1002/admi.202001131.
37. Dhar, N.; Syed, N.; Mohiuddin, M.; Jannat, A.; Zavabeti, A.; Zhang, B.Y.; Datta, R.S.; Atkin, P.; Mahmood, N.; Esrafilzadeh, D.; et al. Exfoliation Behavior of van Der Waals Strings: Case Study of Bi_2S_3. *ACS Appl. Mater. Interfaces* **2018**, *10*, 42603–42611. https://doi.org/10.1021/acsami.8b14702.
38. Yang, D.; Lu, C.; Ma, J.; Luo, M.; Zhao, Q.; Jin, Y.; Xu, X. Enhanced Nonlinear Saturable Absorption from Type III van Der Waals Heterostructure Bi_2S_3/MoS_2 by Interlayer Electron Transition. *Appl. Surf. Sci.* **2021**, *538*, 147989. https://doi.org/10.1016/j.apsusc.2020.147989.
39. Zumeta-Dubé, I.; Ortiz-Quiñonez, J.L.; Díaz, D.; Trallero-Giner, C.; Ruiz-Ruiz, V.F. First Order Raman Scattering in Bulk Bi_2S_3 and Quantum Dots: Reconsidering Controversial Interpretations. *J. Phys. Chem. C* **2014**, *118*, 30244–30252. https://doi.org/10.1021/jp509636n.
40. Clark, R.M.; Kotsakidis, J.C.; Weber, B.; Berean, K.J.; Carey, B.J.; Field, M.R.; Khan, H.; Ou, J.Z.; Ahmed, T.; Harrison, C.J.; et al. Exfoliation of Quasi-Stratified Bi_2S_3 Crystals into Micron-Scale Ultrathin Corrugated Nanosheets. *Chem. Mater.* **2016**, *28*, 8942–8950. https://doi.org/10.1021/acs.chemmater.6b03478.
41. Ni, J.; Bi, X.; Jiang, Y.; Li, L.; Lu, J. Bismuth Chalcogenide Compounds $Bi_2{\times}_3$ (X=O, S, Se): Applications in Electrochemical Energy Storage. *Nano Energy* **2017**, *34*, 356–366. https://doi.org/10.1016/j.nanoen.2017.02.041.
42. Kim, J.; Kwon, S.; Cho, D.H.; Kang, B.; Kwon, H.; Kim, Y.; Park, S.O.; Jung, G.Y.; Shin, E.; Kim, W.G.; et al. Direct Exfoliation and Dispersion of Two-Dimensional Materials in Pure Water via Temperature Control. *Nat. Commun.* **2015**, *6*, 8294. https://doi.org/10.1038/ncomms9294.
43. Ni, P.; Dieng, M.; Vanel, J.C.; Florea, I.; Bouanis, F.Z.; Yassar, A. Liquid Shear Exfoliation of MoS_2: Preparation, Characterization, and NO_2-Sensing Properties. *Nanomaterials* **2023**, *13*, 2502. https://doi.org/10.3390/nano13182502.
44. Medles, M.; Benramdane, N.; Bouzidi, A.; Nakrela, A.; Tabet-Derraz, H.; Kebbab, Z.; Mathieu, C.; Khelifa, B.; Desfeux, R. Optical and Electrical Properties of Bi_2S_3 Films Deposited by Spray Pyrolysis. *Thin Solid Film.* **2006**, *497*, 58–64. https://doi.org/10.1016/j.tsf.2005.09.186.